Molecular mechanisms of seasonal brain shrinkage and regrowth in *Sorex araneus*

William R. Thomas[1]*†, Dina K. N. Dechmann[2,3], John Nieland[4], Cecilia Baldoni[2,3], David Carlson[1], Dominik von Elverfeldt[5], Julie Holm-Jacobsen[4], Marion Muturi[2], Angelique Corthals[6]‡, Liliana M. Dávalos[1,7]‡*

[1]Department of Ecology and Evolution, Stony Brook University; Stony Brook, NY 11794, United States.

[2]Max-Planck Institute for Animal Behavior; Radolfzell, 78315, Germany.

[3]University of Konstanz; Konstanz, 78464, Germany.

[4]Health Science and Technology, Aalborg University; Aalborg, 9100, Denmark.

[5]Department of Diagnostic and Interventional Radiology, University Medical Center Freiburg, Faculty of Medicine, University of Freiburg; Freiburg, 79211, Germany.

[6]John Jay College of Criminal Justice; New York, NY 10019, United States.

[7]Consortium for Inter-Disciplinary Environmental Research, Stony Brook University; Stony Brook, NY 11794, United States.

† Lead author

‡ These authors contributed equally to this work

* Corresponding authors: William R. Thomas and Liliana M. Dávalos

Emails: William.thomas@stonybrook.edu, Liliana.Davalos@stonybrook.edu

Author Contributions: LD, DD, AC, and JN conceived and funded project. CB, MM, and DD collected, measured, and sampled shrews. WRT conducted genomic analyses. WRT, JHJ, JN, and AC analyzed metabolite concentrations. WRT visualized data and wrote initial draft. LD, DD, JN, DC, and AC contributed to review and editing of draft. All authors contributed to data interpretation.

Competing Interest Statement: Authors disclose no competing interests.

Classification: Biological Sciences, Physiology

Keywords: Dehnel's phenomenon, neurodegeneration, winter, metabolism, shrew

Abstract

Human brains typically grow through development, then remain the same size in adulthood, and often shrink through age-related degeneration that induces cognitive decline and impaired functionality. In most cases, however, the neural and organismal changes that accompany shrinkage, especially early in the process, remain unknown. Paralleling neurodegenerative phenotypes, the Eurasian common shrew *Sorex araneus*, shrinks its brain in autumn through winter, but then reverses this process by rapidly regrowing the brain come spring. To identify the molecular underpinnings and parallels to human neurodegeneration of this unique brain size change, we analyzed multi-organ, season-specific transcriptomics and metabolomic data. Simultaneous with brain shrinkage, we discovered system-wide metabolic shifts from lipid to glucose metabolism, as well as neuroprotection of brain metabolic homeostasis through reduced

cholesterol efflux. These mechanisms rely on a finely tuned brain-liver crosstalk that results in changes in expression of human markers of aging and neurodegeneration in Parkinson's disease and Huntington's disease. We propose metabolic shifts with signals that cross the brain blood barrier are central to seasonal brain size changes in *S. araneus*, with potential implications for therapeutic treatment of human neurodegeneration.

Significance Statement

Metabolic regulation has been implicated in altered brain size and function, but the processes that parallel brain shrinkage remain unknown. *Sorex araneus*, the Eurasian common shrew, maintains activity throughout the winter through seasonal brain size plasticity, known as Dehnel's phenomenon. Using this predictable, natural model of brain size change, we generated and analyzed multi-omics data across organs that undergo seasonal size change to characterize underlying molecular mechanisms. Results implicate drastic metabolic shifts and coordinated brain-liver crosstalk in seasonal size change, highlighting the relationship between metabolism, aging, and neurodegeneration.

Main Text

Introduction

Despite the increasing prevalence of neurodegenerative disease (*1*), there are no cures for reversing conditions that impact aging societies worldwide (*2*). One obstacle to finding effective treatments, is that the pathogenesis of most neurodegenerative diseases, especially during early stages, remains obscure. In diseases, such as Parkinson's disease, Alzheimer's disease, and multiple sclerosis, a reduction in brain matter and cognitive or motor decline occurs in tandem with both metabolic dysregulation and inflammatory responses (*3*–*6*). However, the importance of metabolic dysregulation in comparison to other responses in neurodegenerative disorders has been debated (*3*, *7*). These debates are ongoing, as the diagnosis of neurodegenerative disease occurs upon the onset of symptoms, long after initial pathological changes (*1*).

One species, the Eurasian common shrew, *Sorex araneus*, has the potential to illuminate the mechanistic basis of brain decline. *S. araneus* has evolved an extraordinary wintering size plasticity, with a pattern of growth unlike that of almost every other mammal, known as Dehnel's phenomenon (DP) (*8*, *9*). Instead of growing continuously to adulthood, juvenile *S. araneus* grow to an initial maximum size in the first summer of their short life (~1 year). Shrews then shrink, reaching a nadir in winter, followed by rapid regrowth to their adult, breeding size in spring. Extraordinarily, this anticipatory size plasticity also occurs in the brain, with a 26% decrease during winter (*9*), which is then regrown in spring. The benefits of using natural brain size change in *S. araneus* as a model system for human neurodegeneration are twofold. First, we can systematically characterize molecular changes during brain size change, potentially identifying initial pathological changes that predate the winter size minimum. Second, the shrew has the unique capability to regrow brain mass in spring, indicating hitherto unknown restorative mechanisms. Thus, not only can this organismal system shed light on the process of brain shrinkage, it but can also point to potential mechanisms for therapeutic reversal of degeneration in humans.

Based on shrew physiology, we hypothesized that initial declines in brain size are metabolically based, similar to processes implicated in human neurodegenerative diseases. *S. araneus* have one of the highest measured mammalian metabolic rates (*10*). Because of this intrinsic metabolic constraint, DP is an adaptation that anticipates the resource scarcity of winter by decreasing the size of energy-expensive tissue such as the brain (*11*, *12*), which in humans accounts for 20% of glucose metabolized (*13*) and contains 25% of the unesterfied cholesterol found in the body (*14*). Changes in glucose and lipid metabolism have been implicated in the onset of neurodegeneration. For example, circulating insulin and glucose increase in diseases such as type 2 diabetes and obesity, and both are associated with reduced brain size and increased risk of developing Alzheimer's and Parkinson's diseases (*15*–*18*). Thus, seasonal changes in shrew

metabolism may parallel changes associated with metabolic change in human neurodegeneration.

While not excluding neurodegeneration, shrew metabolic shifts could mechanistically resemble other forms of mammalian metabolic plasticity. An alternative wintering strategy, hibernation, involves substantial metabolic changes (*19*, *20*) regulated by a genetic toolkit of metabolic pathways, circadian rhythms, and thermogenesis (*21*). Many of the metabolic changes of wintering strategies are related to the metabolic dysregulation also observed in human neurodegenerative diseases (*22*–*25*). As wintering survival strategies are a continuum of conserved processes (*26*), brain and metabolic alteration in DP could resemble mechanisms of hibernation. However, in contrast with all hibernators, *S. araneus* remain awake throughout the winter season, experiencing a dynamic and hostile environment while actively foraging. This is a key divergence from the mechanisms of hibernation, and instead may involve changes such as reduced lipid metabolism found in hypoxia, which more closely resembles patients with neurodegeneration that also remain active throughout the progression and onset of symptoms.

Testing these alternative hypotheses, we collected transcriptomics, metabolomics, and phenotype data from a shrew population to elucidate how gene expression dynamics change throughout DP. We focused on the liver, where many functions that regulate metabolism take place, including glucose processing, and the brain, where the anticipatory and predictable changes in volume occur. Crucially, our analyses reveal an unequivocal metabolic basis for DP, with implications for age-related human neurodegeneration.

Results

Confirming Dehnel's phenomenon in the German shrew population

Comparisons of body and organ mass throughout the cycle confirmed past findings for patterns of size changes in the brain and spleen, and similar but slightly earlier growth in the liver. (Figure 1B/2A, full results shown in Supplemental Data). Analyzing the 24 shrews collected for all stages of DP (Summer Juvenile=5; Autumn Juvenile n=4; Winter Juvenile n=5; Spring Adult n=5; Summer Adult n=5), we found body mass shrank as expected between Summer Juveniles and Winter Juveniles ($BM_{SuJ-WiJ}$=-1.00g, $p_{SuJ-WiJ}$<0.028), with regrowth as they mature to Spring Adults ($BM_{WiJ-SpA}$=3.724, $p_{WiJ-SpA}$<0.0001). Brain and spleen mass followed the same pattern, as Summer Juveniles reached a minimum by the Winter Juvenile phase ($BrM_{SuJ-WiJ}$=-54.4mg, $p_{SuJ-WiJ}$=0.048; $SpM_{SuJ-WiJ}$=-53.1mg/g of BM, $p_{SuJ-WiJ}$<0.001), with regrowth into Spring Adults ($BrM_{WiJ-SpA}$=71.2mg, $p_{WiJ-SpA}$=.297, $SpM_{WiJ-SpA}$=63.7mg/g of BM, $p_{WiJ-SpA}$<0.01), although not significantly in the brain. Shrew liver mass reached a minimum as Autumn Juveniles ($LiM_{SuJ-AuJ}$=-94.1mg/g of BM, $p_{SuJ-AuJ}$=0.0949). Although regrowth began slightly early as Winter Juveniles ($LiM_{AuJ-WiJ}$=70.4/g of BM, $p_{AuJ-WiJ}$=1.0), the significant portion of regrowth still occurred between the Winter Juvenile and Spring Adult phases ($LiM_{AuJ-SpA}$=607.0mg/g of BM, $p_{WiJ-SpA}$=0.001). Overall, these size changes validated previous research and are further used to guide our transcriptomic characterization of DP.

Reversible metabolic shifts from lipid metabolism to gluconeogenesis during shrinkage

We characterized the plasma metabolome to quantify metabolites throughout the cycle and evaluated the potential shifts in metabolism during shrinkage and regrowth. Of 250 metabolites validated by multiple detection methods in all seasons, we found 28 with significantly different concentrations varying by stage of DP (p<0.05, Figure 1A). Of these differentially concentrated metabolites, three were lipid metabolites; arachidonic acid (p=0.04), ethyl palmitoleate (p=0.02), and docosahexanoic acid (p=0.04). Compared to both Summer Juveniles and Adults, these three lipid metabolites were generally lowest in Autumn Juveniles, Winter Juveniles, and Spring Adults. This indicates limited lipid resource availability as size change occurs and, potentially, suppressed lipid metabolism.

To determine if changes in the metabolome were the result of the regulatory effects of gene expression on size change and suppressed lipid metabolism, we analyzed seasonal variation and differential expression of the metabolically active liver. Instead of resulting from ontogenetic or gradual changes of expression during the shrew lifespan, most of the liver differentially expressed genes (Figure 1C) fell into two temporal clusters, 8 and 12 (Figure 1D), corresponding to genes transiently up- and downregulated during the wintering cycle. Several key transcription factors (*27*, *28*) were differentially expressed mirroring liver size changes, including PPARs, CREBPs, RXRs, and FOXOs. While FOXO1 and FOXO3 promote gluconeogenesis and are reversibly upregulated in Autumn Juveniles, PPARA, PPARD, RXRA, and RXRG are both reversibly downregulated and associated with lipid metabolism (Supplemental Table 1, Figure 1E). All the mentioned liver nutrient sensing transcription factors and the genes they control are differentially expressed mirroring size changes (Supplemental Table 1), indicating large seasonal shifts in metabolism are associated with brain size plasticity. We also identified a single clock gene, PER1, reversibly upregulated in Autumn Juveniles, and an upregulation of genes associated with endocrine signaling (POMC, VDR, NRG1, FGFR4, FGF21). Known to control gene expression and regulate metabolism, differentially expressed liver nutrient sensing, clock transcription factors, and endocrine genes indicate a metabolic switch between from lipid to glucose metabolism during this period of shrinkage and declining circulating lipid availability. This switch parallels mechanisms implicated in evolutionary adaptations to wintering and hypoxia, as well as hypothesized causes of neurodegeneration.

Differential expression analyses focused on genes of high effect, but large modules comprising genes with small effect could also play a pivotal role in regulating seasonal metabolic changes. We characterized interactions in expression among genes and identified modules of co-regulated liver-expressed genes related to seasonal changes in body and liver size using weighted gene co-expression network analysis (WGCNA). We identified 37 modules (Supplemental Figure 2A), of which ten are significantly associated with growth or size changes (Figure 3A). Among these, one module, cyan, encompassed 2,816 genes and correlated with all reversible body and liver size changes. Unlike other modules also significantly associated with summer controls, co-expression in the cyan module is exclusively related to size changes. Therefore, genes in the cyan module are associated with the cyclic shifts that define DP through transient activation and deactivation. In this module, we identified 76 significantly enriched pathways that together form 16 pathway clusters (Figure 3B, Supplemental Data). The most enriched of these pathway clusters comprises four pathways (Figure 3C): insulin resistance, longevity regulating pathway, AMPK signaling pathway, and longevity regulating pathway (across multiple species); and included transcription factors (PPARA, FOXO1, CREB3L2, CREB3L3), their downstream targets (G6PC), PPARG coactivators (PPARGC1A, PPARGC1B), and regulators of inflammation (HNF4A, NFKB1). Therefore, metabolic and longevity-related co-expression in the shrew is associated with these transcription factors, which are also involved in metabolic and age-related progression of neurodegeneration in model organisms.

Decreased brain cholesterol efflux, signatures of neurodegeneration, and a brain-liver axis

We evaluated the effect of metabolic shifts on the shrew brain, which may drive observed size plasticity, while also coordinating seasonal changes in metabolism. First, to disentangle markers of shrinkage from those associated with ontogeny, we compared gene expression across stages in the hippocampus, which shrinks then regrows, and the cortex, which shrinks massively, but experiences minimal regrowth. In the hippocampus, we found 266 differentially expressed genes, only 25 of which were of high effect (Figure 2C). In contrast, the cortex showed 540 differentially expressed genes, with 96 downregulated and 65 upregulated genes of high effect at the Winter Juvenile phase (Figure 2C). Temporal gene clustering analyses revealed fewer distinct clusters in the hippocampus than the liver and cortex, but, as with the liver, most differentially expressed genes are in Clusters 3 and 11, showing transient up and down regulation, consistent with DP (Supplemental Figure 4). For the cortex, most of the high-effect differentially expressed genes grouped in Clusters 1 and 11, with genes in Cluster 1 showing a gradual increase in expression through the life cycle and genes in Cluster 11 being permanently downregulated between the

Autumn Juvenile and Winter Juvenile periods. Despite less variation in gene expression between stages in the brain than in the liver, we identified unique brain-region-specific responses to DP and gene expression patterns consistent with both ontogenetic brain development and DP, especially in the hippocampus.

Testing for differential expression during size change in the hippocampus and cortex, we found few overlapping differentially expressed genes, but both tissue-specific gene sets were enriched for the cholesterol metabolism pathway (Figure 2D), including the apolipoproteins APOA1 and APOH (Figure 2B). In each tissue, the cholesterol metabolism pathway shows a similar trend: cholesterol metabolism upregulated during initial growth and regrowth in the hippocampus, and downregulated during cortex shrinkage, indicating a crucial role of this pathway in both shrinkage and regrowth. Gene co-expression network analyses of the hippocampus also revealed 34 modules (Supplemental Figure 3), three of which correlated with brain shrinkage (Figure 4A). The most significant of these modules (grey) comprised 346 genes, and is associated with both metabolic processes and glycolysis, as well as enriched with genes —such as CASP3, PPARG, CREB3L2, CALM3— in pathways known to underlie neurodegenerative pathogenesis including pathways of neurodegeneration, Parkinson's disease, and Huntington's disease (Figure 4C). Although centered on the key glycolytic enzyme ALDOA (Figure 4B), the regulator of lipid metabolism and transcription factor PPARG is also central to this module. While gene expression patterns in the brain and the liver are distinct, both related through signals of reversible fluctuations in metabolic energy sources. Evidence of both a switch to glucose metabolism in the liver and downregulation of cholesterol metabolism in the brain during shrinkage is consistent with a nadir in circulating lipid metabolites in winter. We therefore propose that concordant shifts in the regulation of lipids in the liver and brain, mirrored by shifting metabolite concentrations in the blood, indicate a pivotal role for regulatory coordination via a brain-liver crosstalk in DP.

Discussion

In humans the early stages of neurodegeneration are difficult to characterize as they may precede symptoms by years, obscuring organismal and neural processes involved in brain shrinkage. With predicable yet reversible brain shrinkage, shrews can be a model of neurodegeneration, but system-wide characterization of their cycle was lacking, precluding insights into the processes that accompany brain shrinkage and regrowth. While metabolic data point to a hypoxia-like state during shrinkage, transcriptomic changes implicate whole-body shifts from lipid to glucose utilization, and brain-specific expression of genes implicated in neurodegeneration. Concurrently, and regulated by a finely tuned brain-liver axis involving signals that cross the blood-brain barrier, the shrew brain appears to decrease cholesterol efflux with potential neuroprotective effect.

If shrew metabolic shifts paralleled hibernation, an increase in lipid metabolites would be observed, but we found autumn, winter, and spring reductions in arachidonic acid, ethyl palmitoleate, and docosahexanoic acid (Figure 1A). Consistent concentration increases of these lipid metabolites have been found in hibernators that shift fuel source from carbohydrates to lipids in winter including the arctic ground squirrel (*29*), hedgehog (*30*), echidna (*31*), brown bear (*19*), and hamster (*32*, *33*). By contrast, shrew metabolite variation during winter more closely resembling conserved hypoxia responses previously found in naked mole rats (*34*), yaks (*35*), and even goldfish (*36*). In hypoxic naked mole rats, stored liver glucose is released into the blood to fuel carbohydrate metabolism (*37*), as the mole rats remain active with only slight reductions in metabolic rate (*38*). Like mole rats in their fossorial environment, shrews stay active throughout the winter and instead of mimicking hibernation, shrew metabolites indicate a hypoxia-like shift to glucose as fuel beginning in autumn shrinkage as lipids become progressively scarcer. We argue this metabolic shift is the foundation of seasonal brain shrinkage.

While metabolomic data implicated hypoxia-like lipid constraints, whether these decreases were mediated by gene regulation was unresolved. By analyzing seasonal differential expression of

metabolically important transcription factors of the liver, we discovered a pivotal switch in autumn shrinkage to a new primary fuel: glucose, which is later reversed in spring. While lipid metabolic genes (e.g., PPARA, PPARD, RXRA, and RXRG) are downregulated, increased PER1 expression signals metabolic demands met by glucose. Indicating this switch, two forehead box transcription factors (FOXOs) associated with glucose metabolism are significantly upregulated during autumn shrinkage (Figure 2C). In mice, FOXO1 and FOXO3 stimulate gluconeogenesis and impede lipid metabolism in response to fasting glucose levels (*28*, *39*–*41*), which promote hepatic glucose production that can be released into the blood for energy utilization throughout the body (*39*, *41*, *42*). Upregulation of these transcription factors in autumn shrews may regulate organismal energy homeostasis via hypoxia-like mechanisms by promoting glucose utilization as lipid metabolism decreases during shrinkage.

FOXO upregulation maintains shrew metabolic homeostasis given challenging environmental conditions and lipid availability, but this incurs costs to both shrew brain size and longevity. The liver co-expression network (cyan) most associated with size change was enriched for genes involved in glucose utilization and longevity associated pathways, which encompassed both *FOXO1* and *SIRT1* (Figure 3). In model organisms including *C. elegans*, *Drosophila*, mice, and humans, FOXO1 dependent glucose utilization and associated PI3K signaling have drastic effects on both body size and lifespan (*43*–*45*). Neurodegeneration is also regarded as an age-related neurological disorder. In the shrew, extreme brain size plasticity in response to metabolic shifts imposed by harsh winters nonetheless comes at a cost to shrew longevity. Compared to other mammals of similar size, *S. araneus* have extraordinarily high metabolic rates (*46*) paired with a short lifespan (*47*) of approximately 13 months. Enrichment of neurodegeneration and longevity pathways in this cyan gene co-expression network further highlights the interplay between metabolic shifts, brain size, and age-related effects, making it a candidate for reversal of degeneration after the onset of neurodegenerative symptoms.

Although these results implicated overall shrew metabolism as a regulator of size plasticity, we sought to identify both the impacts of and effects on the brain. Within the hippocampal gene networks (Figure 4), there was an enrichment of genes centered on the key glycolytic enzyme ALDOA. Associated with neurodegenerative diseases, including Parkinson's and Huntington's disease, *ALDOA* encodes an important enzyme in glycolysis that converts dietary glucose into energy by catalyzing the conversion of fructose biphosphate into glyceraldehyde 3 phosphate (*48*, *49*). Shifts in glucose metabolism during shrew brain shrinkage parallel expression changes in neurodegenerative markers, indicating similar mechanisms underlying both shrew brain shrinkage and human neurodegeneration induced via metabolic change.

Despite these glucose-related changes, we found the shrew's shrinking brain maintains internal lipid homeostasis by reducing cholesterol efflux as a neuroprotective mechanism. Changes in lipid metabolism can occur outside the liver to compensate for energy deficits by self-catabolizing fats (*50*), but maintenance of metabolic homeostasis is important for neural health (*51*, *52*), and self-catabolism in the shrew brain would be extremely detrimental. Except for RXRG, lipid metabolism transcription factors differentially expressed in the liver during seasonal size change (PPARA, PPARB, RXRA) are *not* differentially expressed in the shrew brain. Instead, differential expression analyses indicate limits to brain cholesterol efflux during shrinkage via apolipoproteins (APOs; Figure 2). These signals suggest the shrew brain is protected from bodily lipid constraints during winter food scarcity and instead of self-catabolizing neural fat for energy, the brain responds by limiting cholesterol efflux, conserving function as a neuroprotective mechanism. Neuroprotection has been identified in several other mammals (*53*). For example, naked mole rats have abnormally high concentrations of amyloid beta (*54*), a marker of Alzheimer's disease in humans, but do not develop age-related neurodegenerative diseases (*55*). Thus, cholesterol related markers found in shrews may be protective byproducts of size changes, rather than direct causes of neurodegeneration.

We propose brain-liver crosstalk regulates the shifts in glucose and lipid metabolism in the size-changing liver and brain. Although the brain communicates extrinsic environmental signals to the rest of the body, the blood brain barrier limits the relay of environmental information back to the brain. We identified several gene expression patterns associated with molecules that cross this semi permeable which are involved with brain size change. As circadian clock gene PER1 is downregulated, there is upregulation of genes involved in endocrine signaling in the liver. Endocrine signaling between the brain and liver has been shown to regulate glucose homeostasis (*56*) and are promoted by circadian clock genes (*57*). Additionally, the large liver co-expression module (cyan) of seasonal size change is significantly enriched with AMPK signaling genes in (cyan, Figure 3C). Across mammals, AMPK signaling restores energy balance by transitioning between anabolic and catabolic pathways in response to circulating glucose levels (*58*, *59*) through tissue-specific cross-modulation. In shrews, liver-specific change in AMPK signaling, in tandem with circadian and endocrine signaling, modulate both brain and liver expression changes in response to the transition from lipids to glucose as a fuel source.

Coordinated changes in gene expression of the liver and brain, the proposed brain-liver axis, are ideal candidate mechanisms of brain shrinkage. Functional relationships, or axes, as the brain receives stimuli from peripheral tissues have been shown to induce vast changes in brain function, expression, and phenotype. These stimuli range from inflammatory responses sent from the spleen (*60*) to regulation of nutrient metabolism through gut microbiota signals (*61*). In mammals, alterations to the brain-liver axis have been implicated in several models of neurodegenerative disease (*62*–*65*). For example, in mice models of Parkinson's disease, nigrostriatal degeneration results in hepatic mitochondrial dysfunction, causing metabolic dysregulation that self-perpetuates initial neurodegenerative symptoms (*63*). Reversals of candidate genes and pathways within this brain-liver axis, however, indicate these processes may not be self-perpetuating as found in Parkinson's disease models. Instead, the reversals suggest an effective self-regulatory mechanism that not only causes shrinkage, but also allows brain regrowth. Expression reversals via the brain-liver axis are exemplary candidates for therapeutic treatments.

We characterized the unique brain shrinkage and regrowth in the common shrew, as defining the molecular mechanisms of this brain plasticity is of crucial importance to establish DP in the *S. araneus* as a model for mammalian neurodegeneration. Stage-by-stage analysis of liver RNA expression identified an early-onset change: a metabolic switch from lipid to glucose metabolism during shrinkage derived from lipid constraints, yet reversible during regrowth. In the shrew brain, this switch is accompanied by neuroprotective mechanisms —decreased cholesterol efflux—, and correlations with pathways associated with neurodegenerative disease. This shift in brain and liver metabolism appears to be regulated by circadian clock genes and key transcription factors that promote signals that can permeate into the brain. In conclusion, we propose these changes indicate a crosstalk between the brain and liver that underlies metabolic and seasonal brain size change, including candidate genes and pathways with numerous implications for longevity, neurodegenerative prognosis, and therapeutic treatments of age-related neurodegenerative diseases.

Materials and Methods

Further details of experimental protocols are described in SI Appendix. Code and data can be found on GitHub: https://github.com/wrthomas315/Dehnels_Seasonal_RNAseq/tree/main/data

Sample Collection and RNA Sequencing

European common shrews were trapped with insulated wooden traps in Radolfzell, Germany, at five different stages of development: Summer Juveniles (n=5), Autumn Juveniles (n=4), Winter Juveniles (n=5), Spring Adults (n=5), and Summer Adults (n=5). Shrews were aged and sexed based on tooth wear, fur appearance, and gonad development prior to euthanasia. Blood serum was collected through the heart, let stand for 15 minutes, spun down at 1200rpm, and then stored

at -80°C. Shrews were then euthanized by perfusion via the vascular system with PAXgene Tissue Fixative. All organs were removed and weighed to confirm the occurrence of DP for each organ using a t-test between stages. Thoracic organs were placed immediately into PAXgene Tissue Stabilizer, while the brain was submerged in cold fixative and dissected into each region, and then placed into PAXgene Tissue Stabilizer. Samples were then placed in stabilizer (2-24 hours later) and then stored in liquid nitrogen. RNA was extracted with a modified Qiagen Micro RNAeasy protocol used for small amounts of mammalian sensory tissue. Tissues extracted included the liver, neocortex, and hippocampus. RNA was sent to Genewiz for quality control, library preparation, and sequencing. Quantity of RNA was measured with a Nanodrop spectrophotometer and quality of RNA assessed with RNA ScreenTape. Libraries were prepared with standard polyA selection and sequenced as 150bp pair-end reads for a target of 15-25 million reads per sample.

Differential Gene Expression Analysis

We trimmed adapters and filtered reads using fastp (*66*) and removed samples with extreme read counts (~10-fold). Gene counts were quantified by pseudo aligning to the 19,296 protein coding genes of the *S. araneus* genome (sorAra2; GCF_000181275.1) using Kallisto (*67*). Tests for differential gene expression were conducted between the phenotypically extreme stages of the same tissue. For the liver, Autumn Juveniles and Spring Adults were compared, which also overlap with the spleen, hippocampus, and cortex shrinking and regrowth phases, such that we could make inferences about potential extrahepatic signals. Winter Juveniles (hippocampus minimum) and Spring Adults (hippocampus regrowth) were compared. For the cortex, Summer Juveniles (before shrinkage) and Winter Juveniles (cortex minimum) were compared, as the cortex does not enter a period of substantial regrowth (*9*). Counts were normalized for each tissue using DESeq2 (*68*) median of ratios. Each gene was fitted with a negative binomial generalized linear model and then we used a Wald test to examine if differences in gene expression was the result of the season parameter, with p-values corrected using the Benjamini and Hochberg procedure (*69*). To identify how many significant differentially expressed genes were of high effect for gene set enrichments, and to reduce the number of genes to improve interpretability, we filtered significant results for genes higher and lower than 1.58 log-fold change (absolute 3-fold change). The hippocampus data had very few differentially expressed genes when filtered (n=25), and log-fold change filtering was omitted for this tissue. We then identified enriched KEGG Gene Ontology (GO) pathways in the gene data sets using DAVID functional annotation (*70*).

Temporal Clustering

We used our normalized gene expressions to also analyze gene expression through time using the package TCseq (*71*). To remove genes with relatively little change in expression, we filtered each organ set for genes with an absolute fold change less than 0.5 between any two stages. Next, we filtered any gene with extremely low expression, such that two samples had to have greater than ten normalized reads. We then transformed each gene expression profile across stages to z-scores, and then used fuzzy cmeans clustering to identify clusters of similar gene expression profiles. The number of resultant gene clusters was found by bootstrapping (n=20) a gap statistic that minimized the within-cluster distance (standard error from center). Finally, we took the high-effect significant results from differential analysis and identified each gene's maximum degree of cluster membership.

Weighted Gene Co-expression Network Analysis

We used the WGCNA package (*72*) package to create co-expression networks for the liver and hippocampus and determined if these correlations between genes are significantly correlated with our shrinkage and regrowth phenotypes. Network construction parameters and code can be found in the SI Appendix and on GitHub. Cytoscape (*73*) was used to visualize significant networks and calculate network statistics such as node (gene) connectivity. Identification of

potential function of each module were analyzed using DAVID Gene Functional Classification Tool to test for GO enrichment (*70*).

Metabolomics
Metabolite analysis was carried out by MS-Omics using a Thermo Scientific Vanquish LC (UPLC) coupled to Thermo Q Exactive HF MS. Identification of compounds were performed at four levels; Level 1: identification by retention times (compared against in-house authentic standards), accurate mass (with an accepted deviation of 3ppm), and MS/MS spectra, Level 2a: identification by retention times (compared against in-house authentic standards), accurate mass (with an accepted deviation of 3ppm). Level 2b: identification by accurate mass (with an accepted deviation of 3ppm), and MS/MS spectra. MetaboAnalyst was used to test for changes in concentration between seasons (*74*). Concentrations for each sample were normalized by the average concentration of our Summer Adults samples and log transformed and auto scaled. A one-way ANOVA was used to test for any significant seasonal difference in metabolite concentration, with p-values corrected with an false discovery rate of 0.05. Within each significant metabolite, t-tests were used to identify pairwise differences in mean between each season. Samples were hierarchically clustered using significant genes and visualized using a heatmap.

Acknowledgments
We thank Joshua Rest, Krishna Veeramah, and Tanya Lama who have provided helpful feedback on initial results and previous versions of the manuscript. We thank Michal Oklinski for help with initial dissections.

Funding
WRT and research were supported by the Human Frontiers in Science Program Award (RGP0013/2019) to DD, LMD, and JN

References
1. J. C. Zheng, S. Chen, Translational Neurodegeneration in the era of fast growing international brain research. *Transl. Neurodegener.* **11**, 10–11 (2022).
2. B. L. Swenson, C. F. Meyer, T. J. Bussian, D. J. Baker, Senescence in aging and disorders of the central nervous system. *Transl. Med. Aging*. **3**, 17–25 (2019).
3. A. P. Corthals, Multiple sclerosis is not a disease of the immune system. *Q. Rev. Biol.* **86**, 287–321 (2011).
4. P. Gamba *et al*., A crosstalk between brain cholesterol oxidation and glucose metabolism in Alzheimer's disease. *Front. Neurosci.* **13**, 1–9 (2019).
5. U. Jin, S. J. Park, S. M. Park, Cholesterol metabolism in the brain and its association with Parkinson's disease. *Exp. Neurobiol.* **28**, 554–567 (2019).
6. C. K. Glass, K. Saijo, B. Winner, M. C. Marchetto, F. H. Gage, Mechanisms Underlying Inflammation in Neurodegeneration. *Cell*. **140**, 918–934 (2010).
7. J. M. Greer, P. A. McCombe, Role of gender in multiple sclerosis: Clinical effects and potential molecular mechanisms. *J. Neuroimmunol.* **234**, 7–18 (2011).
8. Z. Pucek, Seasonal and age changes in the weight of internal organs of shrews. *Acta Theriol. (Warsz).* **10**, 369–438 (1965).
9. J. Lázaro, M. Hertel, C. C. Sherwood, M. Muturi, D. K. N. Dechmann, Profound seasonal changes in brain size and architecture in the common shrew. *Brain Struct. Funct.* **223**, 2823–2840 (2018).
10. M. Genoud, K. Isler, R. D. Martin, Comparative analyses of basal rate of metabolism in mammals : data selection does matter. *Biol. Rev.* **93**, 404–438 (2018).
11. J. Lázaro, M. Hertel, M. Muturi, D. K. N. Dechmann, Seasonal reversible size changes in the braincase and mass of common shrews are flexibly modified by environmental conditions. *Sci. Rep.* **9**, 1–10 (2019).
12. L. Keicher, M. T. O'Mara, C. C. Voigt, D. K. N. Dechmann, Stable carbon isotopes in breath reveal fast metabolic incorporation rates and seasonally variable but rapid fat

turnover in the common shrew (Sorex araneus). *J. Exp. Biol.* **220**, 2834–2841 (2017).
13. P. Mergenthaler, U. Lindauer, G. A. Dienel, A. Meisel, Sugar for the brain: The role of glucose in physiological and pathological brain function. *Trends Neurosci.* **36**, 587–597 (2013).
14. D. A. Elliott, C. S. Weickert, B. Garner, Apolipoproteins in the brain: Implications for neurological and psychiatric disorders. *Clin. Lipidol.* **5**, 555–573 (2010).
15. R. Agrawal, F. Gomez-Pinilla, "Metabolic syndrome" in the brain: Deficiency in omega-3 fatty acid exacerbates dysfunctions in insulin receptor signalling and cognition. *J. Physiol.* **590**, 2485–2499 (2012).
16. H. Macpherson, M. Formica, E. Harris, R. M. Daly, Brain functional alterations in Type 2 Diabetes – A systematic review of fMRI studies. *Front. Neuroendocrinol.* **47**, 34–46 (2017).
17. C. Sims-Robinson, B. Kim, A. Rosko, E. L. Feldman, How does diabetes accelerate Alzheimer disease pathology? *Nat. Rev. Neurol.* **6**, 551–559 (2010).
18. D. Wang *et al*., A mouse model for Glut-1 haploinsufficiency. *Hum. Mol. Genet.* **15**, 1169–1179 (2006).
19. B. Chazarin *et al*., Metabolic reprogramming involving glycolysis in the hibernating brown bear skeletal muscle. *Front. Zool.* **16**, 1–21 (2019).
20. J. L. Villanueva-Cañas, S. L. Faherty, A. D. Yoder, M. M. Albà, Comparative genomics of mammalian hibernators using gene networks. *Integr. Comp. Biol.* **54**, 452–462 (2014).
21. S. L. Faherty, J. Luis Villanueva-Cañas, P. H. Klopfer, M. M. Albà, A. D. Yoder, Gene expression profiling in the hibernating primate, Cheirogaleus medius. *Genome Biol. Evol.* **8**, 2413–2426 (2016).
22. J. A. Davis *et al*., High-Fat and High-Sucrose Diets Impair Time-of-Day Differences in Spatial Working Memory of Male Mice. *Obesity*. **28**, 2347–2356 (2020).
23. A. Jayaraman, D. Lent-Schochet, C. J. Pike, Diet-induced obesity and low testosterone increase neuroinflammation and impair neural function. *J. Neuroinflammation*. **11**, 1–14 (2014).
24. M. P. Mattson, T. V. Arumugam, Hallmarks of Brain Aging: Adaptive and Pathological Modification by Metabolic States. *Cell Metab.* **27**, 1176–1199 (2018).
25. A. Mondal *et al*., Lipocalin 2 induces neuroinflammation and blood-brain barrier dysfunction through liver-brain axis in murine model of nonalcoholic steatohepatitis. *J. Neuroinflammation*. **17**, 1–15 (2020).
26. G. G. Auteri, L. L. Knowles, Decimated little brown bats show potential for adaptive change. *Sci. Rep.* **10**, 1–10 (2020).
27. P. Nguyen *et al*., Liver lipid metabolism. *J. Anim. Physiol. Anim. Nutr. (Berl).* **92**, 272–283 (2008).
28. Z. Yang, K. Roth, M. Agarwal, W. Liu, M. C. Petriello, The transcription factors CREBH, PPARa, and FOXO1 as critical hepatic mediators of diet-induced metabolic dysregulation. *J. Nutr. Biochem.* **95**, 108633 (2021).
29. S. A. Rice *et al*., Omega 3 fatty acids stimulate thermogenesis during torpor in the Arctic Ground Squirrel. *Sci. Rep.* **11**, 1–14 (2021).
30. S. Laukola, Seasonal changes in the fatty acid spectrum of the hedgehog's white and brown adipose tissue. *Ann. Zool. Fennici*. **17**, 191–201 (1980).
31. F. Falkenstein, G. Körtner, K. Watson, F. Geiser, Dietary fats and body lipid composition in relation to hibernation in free-ranging echidnas. *J. Comp. Physiol. - B Biochem. Syst. Environ. Physiol.* **171**, 189–194 (2001).
32. S. Giroud *et al*., Membrane Phospholipid Fatty Acid Composition Regulates Cardiac SERCA Activity in a Hibernator, the Syrian Hamster (Mesocricetus auratus). *PLoS One*. **8** (2013), doi:10.1371/journal.pone.0063111.
33. F. Geiser, M. Klingenspor, B. M. McAllan, A Functional Nexus between Photoperiod Acclimation, Torpor Expression and Somatic Fatty Acid Composition in a Heterothermic Mammal. *PLoS One*. **8** (2013), doi:10.1371/journal.pone.0063803.
34. M. R. Pergande *et al*., PPARα and PPARγSignaling Is Enhanced in the Brain of the Naked

Mole-Rat, a Mammal that Shows Intrinsic Neuroprotection from Oxygen Deprivation. *J. Proteome Res.* **20**, 4258–4271 (2021).
35. X. Meng *et al*., UPLC-QTOF/MS-based metabolomic analysis of plasma reveals altitude effects on yaks (Bos grunniens). *Thai J. Vet. Med.* **51**, 551–559 (2021).
36. E. Farhat, E. D. Turenne, K. Choi, J. M. Weber, Hypoxia-induced remodelling of goldfish membranes. *Comp. Biochem. Physiol. Part B*. **237**, 1–8 (2019).
37. M. E. Pamenter, Adaptations to a hypoxic lifestyle in naked mole-rats. *J. Exp. Biol.* **225** (2022), doi:10.1242/jeb.196725.
38. A. M. Kirby, G. D. Fairman, M. E. Pamenter, Atypical behavioural, metabolic and thermoregulatory responses to hypoxia in the naked mole rat (Heterocephalus glaber). *J. Zool.* **305**, 106–115 (2018).
39. W. Zhang *et al*., FoxO1 regulates multiple metabolic pathways in the liver effects on gluconeogenic, glycolytic, and lipogenic gene expression. *J. Biol. Chem.* **281**, 10105–10117 (2006).
40. I. Tikhanovich, J. Cox, S. A. Weinman, Forkhead box class O transcription factors in liver function and disease. *J. Gastroenterol. Hepatol.* **28**, 125–131 (2013).
41. X. Xiong, R. Tao, R. A. DePinho, X. C. Dong, Deletion of Hepatic FoxO1/3/4 Genes in Mice Significantly Impacts on Glucose Metabolism through Downregulation of Gluconeogenesis and Upregulation of Glycolysis. *PLoS One*. **8**, 1–11 (2013).
42. M. Matsumoto, A. Pocai, L. Rossetti, R. A. DePinho, D. Accili, Impaired Regulation of Hepatic Glucose Production in Mice Lacking the Forkhead Transcription Factor Foxo1 in Liver. *Cell Metab.* **6**, 208–216 (2007).
43. M. S. Gami, C. A. Wolkow, Studies of Caenorhabditis elegans DAF-2/insulin signaling reveal targets for pharmacological manipulation of lifespan. *Aging Cell*. **5**, 31–37 (2006).
44. D. S. Hwangbo, B. Garsham, M. P. Tu, M. Palmer, M. Tatar, Drosophila dFOXO controls lifespan and regulates insulin signalling in brain and fat body. *Nature*. **429**, 562–566 (2004).
45. A. Satoh *et al*., Sirt1 extends life span and delays aging in mice through the regulation of Nk2 Homeobox 1 in the DMH and LH. *Cell Metab.* **18**, 416–430 (2013).
46. J. R. E. Taylor, Evolution of Energetic Strategies in Shrews. *Evol. Shrews*, 309–346 (1998).
47. K. Healy *et al*., Ecology and mode-of-life explain lifespan variation in birds and mammals. *Proc. R. Soc. B Biol. Sci.* **281** (2014), doi:10.1098/rspb.2014.0298.
48. S. Du *et al*., Fructose-bisphosphate aldolase a is a potential metastasis-associated marker of lung squamous cell carcinoma and promotes lung cell tumorigenesis and migration. *PLoS One*. **9** (2014), doi:10.1371/journal.pone.0085804.
49. J. H. T. Potter *et al*., Nectar-feeding bats and birds show parallel molecular adaptations in sugar metabolism enzymes. *Curr. Biol.* **31**, 1–8 (2021).
50. C. N. Brocker *et al*., Extrahepatic PPAR modulates fatty acid oxidation and attenuates fasting-induced hepatosteatosis in mice. *J. Lipid Res.* **59**, 2140–2152 (2018).
51. D. Val-Laillet, S. Layec, S. Guérin, P. Meurice, C. H. Malbert, Changes in brain activity after a diet-induced obesity. *Obesity*. **19**, 749–756 (2011).
52. R. Agrawal *et al*., Deterioration of plasticity and metabolic homeostasis in the brain of the UCD-T2DM rat model of naturally occurring type-2 diabetes. *Biochim. Biophys. Acta - Mol. Basis Dis.* **1842**, 1313–1323 (2014).
53. K. R. Dave, S. L. Christian, M. A. Perez-Pinzon, K. L. Drew, Neuroprotection: Lessons from hibernators. *Comp. Biochem. Physiol. - B Biochem. Mol. Biol.* **162**, 1–9 (2012).
54. D. Frankel *et al*., Cholesterol-rich naked mole-rat brain lipid membranes are susceptible to amyloid beta-induced damage in vitro. *Aging (Albany. NY).* **12**, 22266–22290 (2020).
55. Y. H. Edrey *et al*., Amyloid beta and the longest-lived rodent: The naked mole-rat as a model for natural protection from alzheimer's disease. *Neurobiol. Aging*. **34**, 2352–2360 (2013).
56. A. Kalsbeek *et al*., Circadian control of the daily plasma glucose rhythm: An interplay of GABA and glutamate. *PLoS One*. **3** (2008), doi:10.1371/journal.pone.0003194.

57. F. Gachon, U. Loizides-Mangold, V. Petrenko, C. Dibner, Glucose homeostasis: Regulation by peripheral circadian clocks in rodents and humans. *Endocrinology*. **158**, 1074–1084 (2017).
58. S.-C. Lin, D. G. Hardie, AMPK: Sensing Glucose as well as Cellular Energy Status. *Cell Metab.* **27**, 299–313 (2018).
59. Y. Minokoshi *et al*., AMP-kinase regulates food intake by responding to hormonal and nutrient signals in the hypothalamus. *Nature*. **428**, 569–574 (2004).
60. B. Zhang, J. Zhong, Z. Gao, A Brain-Spleen Axis Regulates Humoral Immunity. *Neurosci. Bull.* **37**, 427–429 (2021).
61. S. Z. Wang, Y. J. Yu, K. Adeli, Role of gut microbiota in neuroendocrine regulation of carbohydrate and lipid metabolism via the microbiota-gut-brain-liver axis. *Microorganisms*. **8**, 8–10 (2020).
62. N. Zeltser *et al*., Neurodegeneration in juvenile Iberian pigs with diet-induced nonalcoholic fatty liver disease. *Am. J. Physiol. - Endocrinol. Metab.* **319**, E592–E606 (2020).
63. M. Vairetti *et al*., Impaired hepatic function and central dopaminergic denervation in a rodent model of Parkinson's disease: A self-perpetuating crosstalk? *Biochim. Biophys. Acta - Mol. Basis Dis.* **1822**, 176–184 (2012).
64. Z. Huang, H. W. Lin, Q. Zhang, X. Zong, Targeting Alzheimer's Disease: The Critical Crosstalk between the Liver and Brain. *Nutrients*. **14** (2022), doi:10.3390/nu14204298.
65. M. Trapecar *et al*., Human physiomimetic model integrating microphysiological systems of the gut, liver, and brain for studies of neurodegenerative diseases. *Sci. Adv.* **7** (2021), doi:10.1126/SCIADV.ABD1707.
66. S. Chen, Y. Zhou, Y. Chen, J. Gu, Fastp: An ultra-fast all-in-one FASTQ preprocessor. *Bioinformatics*. **34**, i884–i890 (2018).
67. N. L. Bray, H. Pimentel, P. Melsted, L. Pachter, Near-optimal probabilistic RNA-seq quantification. *Nat. Biotechnol.* **34**, 525–527 (2016).
68. M. I. Love, W. Huber, S. Anders, Moderated estimation of fold change and dispersion for RNA-seq data with DESeq2. *Genome Biol.* **15**, 1–21 (2014).
69. Y. Benjamini, Y. Hochberg, Controlling the False Discovery Rate : A Practical and Powerful Approach to Multiple Testing. *J. R. Stat. Soc.* **57**, 289–300 (1995).
70. D. W. Huang, B. T. Sherman, R. A. Lempicki, Systematic and integrative analysis of large gene lists using DAVID bioinformatics resources. *Nat. Protoc.* **4**, 44–57 (2009).
71. L. G. Mengjun, TCseq: Time course sequencing data analysis. R package version 1.8.0., 1–8 (2019).
72. P. Langfelder, S. Horvath, WGCNA: An R package for weighted correlation network analysis. *BMC Bioinformatics*. **9** (2008), doi:10.1186/1471-2105-9-559.
73. P. Shannon *et al*., Cytoscape: A Software Environment for Integrated Models. *Genome Res.* **13**, 2498–2504 (2003).
74. Z. Pang *et al*., MetaboAnalyst 5.0: Narrowing the gap between raw spectra and functional insights. *Nucleic Acids Res.* **49**, 388–396 (2021).

Figures

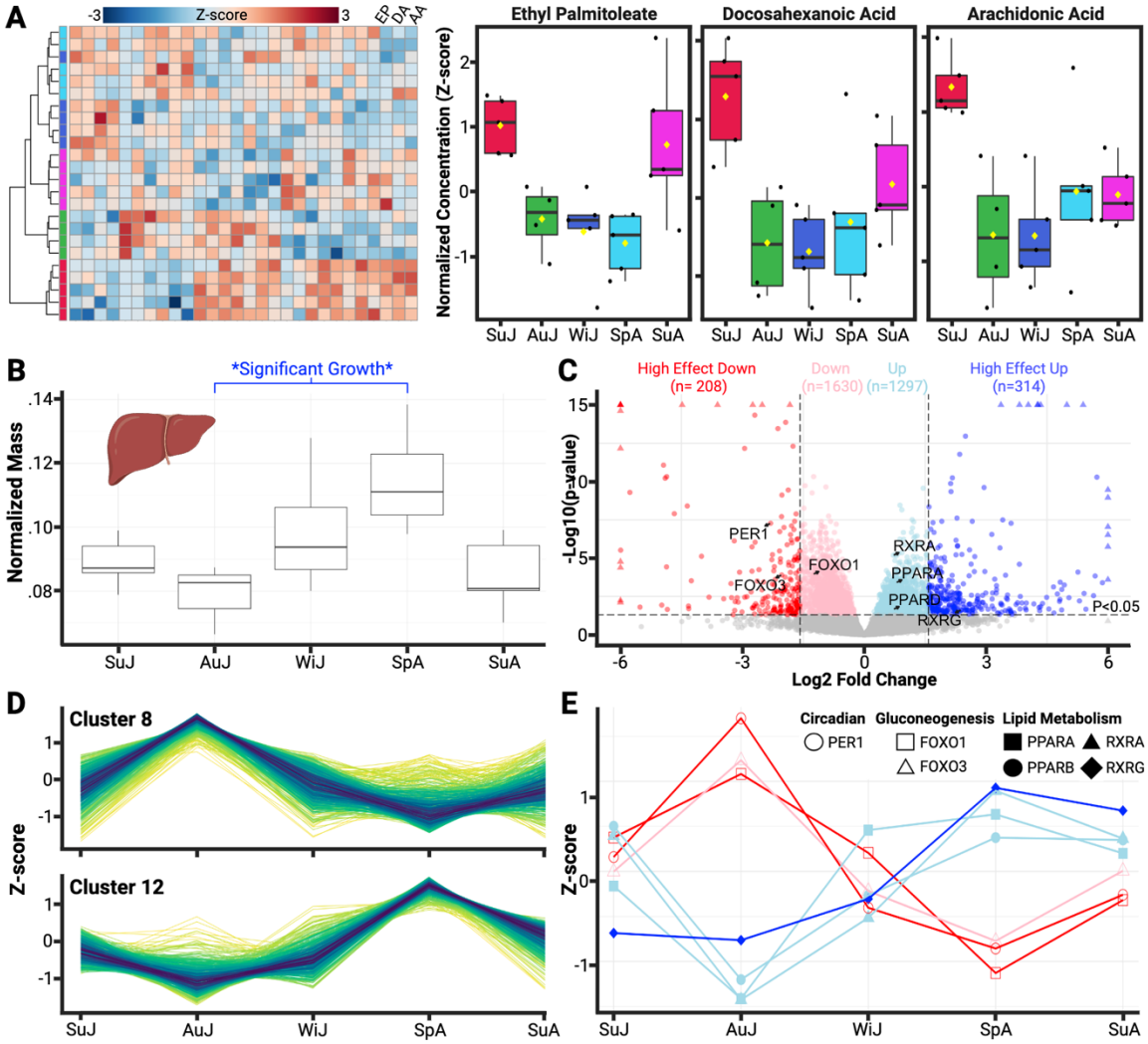

Figure 1. Metabolic profiling of the blood metabolome and liver transcriptomes. (**A)** Heatmap of 28 statistically significant differentially concentrated metabolites between stages of Dehnel's phenomenon. Hierarchical clustering using these significant metabolites groups each profile into each season. Three of these metabolites were lipid metabolites (ethyl palmitoleate, docosahexanoic acid, arachidonic acid), with decreases in autumn, winter, and spring individuals. **(B)** Mass change in liver through five stages of Dehnel's phenomenon. Unlike other organs, the liver reaches a minimum as an Autumn Juvenile, with regrowth beginning as a Winter Juvenile. Asterisks represent significant size changes (adjusted $p<0.05$). **(C)** Volcano plot of significant (adjusted $p<0.05$) differentially expressed genes (colored) between phenotypic extremes of liver size change (Spring Adult vs Autumn Juvenile) plotted by log fold-change. Vertical thresholds represent a 1.58 log fold-change in differential expression of high effect between stages (dark colors). **(D)** Temporal gene expression clusters 8 and 12, most significant differentially expressed genes. **(E)** Patterning of gene expression across stages of Dehnel's phenomenon for transcription factors pivotal roles in lipid metabolism and gluconeogenesis. Lipid metabolism and gluconeogenesis appear to have inverse cycles, with lipid metabolism decreasing in the fall and increasing in the spring, with gluconeogenesis following the opposite trend.

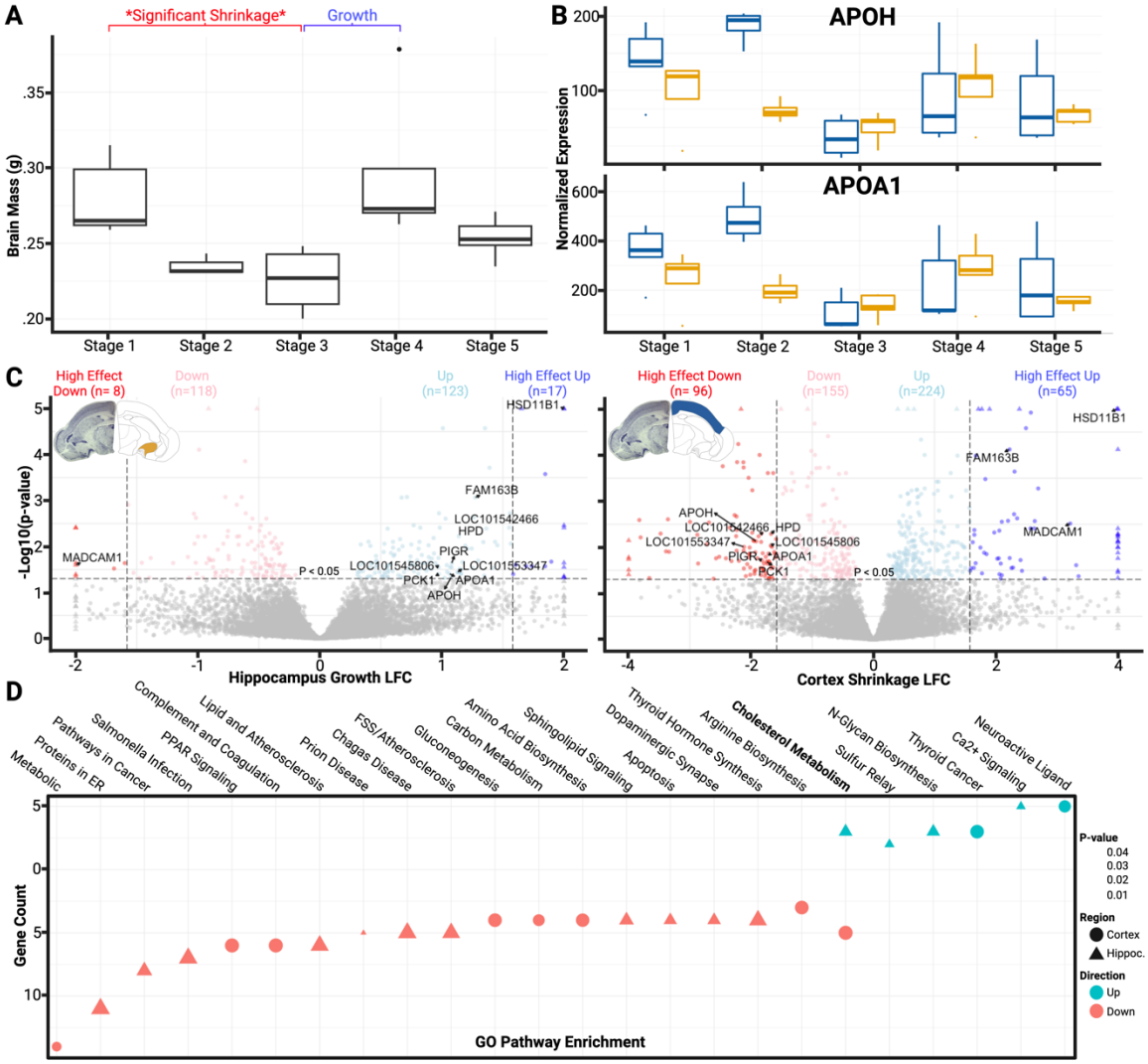

Figure 2. Seasonal plasticity in brain phenotype and expression patterns. **(A)** Brain mass change through five stages of Dehnel's phenomenon. As does body mass, the brain begins to shrink as Autumn Juveniles, reaching a minimum as Winter Juveniles, and regrows as Spring Adults. Asterisks represent significant size changes (adjusted p<0.05). **(B)** 11 genes were differentially expressed in both brain regions, including the apolipoproteins APOA1 and APOH, which both show winter decreases followed by slight spring upregulation. **(C)** Volcano plot of significant (adjusted p<0.05) differentially expressed genes (colored) in *hippocampal regrowth* (Spring Adults vs Winter Juveniles) and *cortex shrinkage* (Winter Juveniles vs Summer Juveniles) plotted by log fold-change. Vertical thresholds represent a 1.58 log fold-change which show differential expression of high effect between stages. **(D)** APOA1 and APOH are found in the cholesterol metabolism pathway, which was enriched for differentially expressed genes in both shrinkage and regrowth phenotypes.

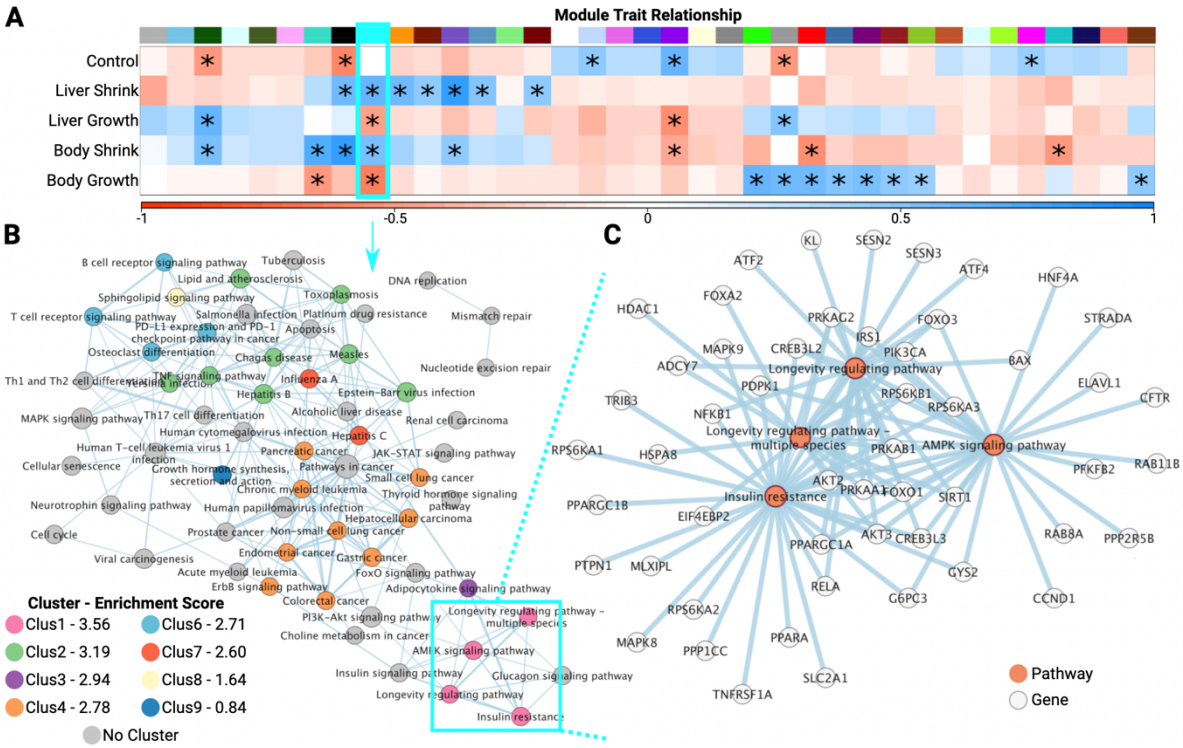

Figure 3. Gene network analyses across liver and body phenotypes of Dehnel's phenomenon. (**A**) Modules (n=37) of high gene co-expression in the liver, including 21 modules with significant correlation with at least one change phenotype (Controls, Liver Shrinkage, Liver Growth, Body Shrinkage, and Body Growth). The 2816 gene cyan module was significant in all size changes, tests for pathway enrichment found 77 significantly enriched pathways, with 59 shown after filtering (removed pathways without 2 neighbors for simplicity). (**B**) Gene pathways clustered in 16 clusters GO-pathways based on gene similarity (**C**) Cluster 1 was the most enriched cluster (Enrichment Score 3.56; higher ES occurs with lower geometric mean of encompassed pathway p-values) containing four pathways; Insulin resistance, Longevity regulating pathway, AMPK signaling pathway, and Longevity regulating pathway-multiple species.

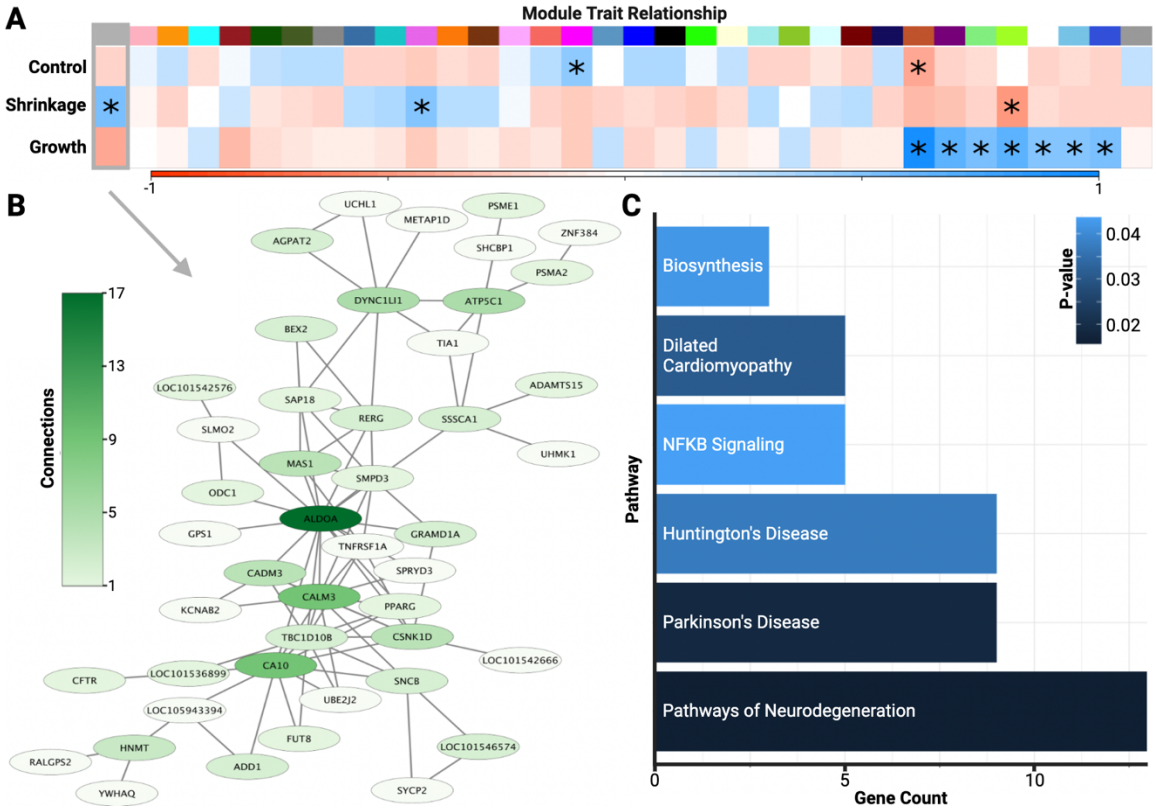

Figure 4. Gene network analyses across hippocampal size change. (**A**) Modules (34) of high gene co-expression in the hippocampus, including ten modules significantly correlated with target phenotypes (Regrowth, Shrinkage, and Control). The 346 gene grey module was the most significant module associated within the shrinkage phenotype ($p = 0.01$, $r = 0.55$). (**B**) Visualization of gene network (filtered and removed edges with weighted correlations < 0.02 and nodes with only a single neighbor). ALDOA was the most central to the network, with 17 connections to other nodes. (**C**) Pathway enrichment analysis also identified 6 pathways to be enriched for genes in the grey module: Pathways of Neurodegeneration, Parkinson's disease, Huntington's disease, NF-kappa beta Signaling, Dilated Cardiomyopathy, and Biosynthesis.